

To be published in the *Astronomical Journal*, July 1999

# Determination of Galaxy Spin Vectors in the Pisces-Perseus Supercluster with the Arecibo Telescope

J. E. Cabanela and John M. Dickey

Astronomy Department, University of Minnesota  
116 Church Street SE, Minneapolis, MN 55455

## ABSTRACT

We use HI observations made with the upgraded Arecibo 305M Telescope in August 1998 to obtain accurate spin vector determinations for 54 nearly edge-on galaxies in the Minnesota Automated Plate Scanner Pisces-Perseus Survey (MAPS-PP). We introduce a simple observational technique of determining the sense of rotation for galaxies, even when their HI disks are not fully resolved. We examined the spin vector distribution of these 54 galaxies for evidence of preferential galaxy alignments. We use the Kuiper statistic, a variant of the Kolmogorov–Smirnov statistic, to determine the significance of any anisotropies in the distribution of galaxy spin vectors. The possibility of “spin vector domains” is also investigated. We find no significant evidence of preferential galaxy alignments in this sample. However, we show that the small sample size places weak limits on the level of galaxy alignments.

*Subject headings:* galaxies:formation — large-scale structure

## 1. Introduction

The search for galaxy alignments has a long history, beginning with searches for alignments in “Spiral and Elliptical Nebulae” during the late 19th Century. Recent scrutiny of the problem has been motivated by the understanding that establishing the level of galaxy spin vector ( $\vec{L}$ ) alignments could offer an additional constraint on various theories of galaxy formation and evolution. For example, “top-down” scenarios of Large-Scale Structure formation can lead to ordered distributions of angular momentum on cluster and supercluster scales through a variety of mechanisms (Zel’dovich 1970, Doroshkevich &

Shandarin 1978, White 1984, Colberg, *et al.* 1998). In addition to galaxy  $\vec{L}$  alignments resulting from various formation mechanisms, galaxy  $\vec{L}$  alignments may also be the evolutionary result of anisotropic merger histories (West 1994), galaxy-galaxy interactions (Sofue 1992), or strong gravitational gradients (Ciotti & Dutta 1994, Ciotti & Giampieri 1998). For a summary of the history of the field, see Djorgovski (1987) and Cabanela & Aldering (1998) [hereafter Paper I].

Observational support exists for some forms of galaxy  $\vec{L}$  alignments with surrounding large-scale structure. For example, Binggeli (1982) discovered that the major axes of cD galaxies tended to be aligned with the axes of their parent cluster. However, most previous searches for galaxy alignments have had results that one could describe as negative or statistically significant but not strongly so. One complication in earlier efforts has been that most have not truly determined  $\vec{L}$ , but rather simply used the position angle (and sometimes ellipticity) of the galaxies in an attempt to determine the possible distribution of  $\vec{L}$ . However, for each combination of galaxy position angle and ellipticity, there are four solutions for the true orientation of the galactic angular momentum axis ( $\vec{L}$ ). This degeneracy in  $\vec{L}$  can only be removed by establishing both which side of the major axis is moving toward the observer and whether we are viewing the north or south side of the galaxy, where “north” is in the direction the galaxy angular momentum vector. Therefore previous studies have either restricted themselves to using only position angles of galaxies, or they have often taken all four possible solutions of  $\vec{L}$  with equal weight (Flin 1988, Kashikawa & Okamura 1992).

Several studies have been published regarding searches for alignments using completely determined galaxy angular momentum axes. Helou & Salpeter (1982) used HI and optical observations of 20 galaxies in the Virgo cluster to show that no very strong  $\vec{L}$  alignments exist. However, a followup to this study by Helou (1984) found evidence for anti-alignments of spin vectors for binary pairs of galaxies in a sample of 31 such pairs. Hoffman *et al.* (1989) briefly investigated the possibility of galaxy alignments by plotting up the  $\vec{L}$  orientations for  $\sim 85$  galaxies with fully determined spin vectors from their Virgo cluster sample and found no obvious alignments. Most recently, Han, Gould, & Sackett (1995) used a sample of 60 galaxies from the Third Reference Catalogue of Bright Galaxies (de Vaucouleurs *et al.* 1991, hereafter referred to as the RC3) in the “Ursa Major filament” and found no evidence of galaxy alignments.

There are several criticisms one can level against these earlier studies. All the studies attempted to use relatively small samples to map out orientation preferences over the entire sky. Thus only very strong  $\vec{L}$  alignment signatures could have been discovered via this method. The samples were selected using source catalogs with “visual” criteria which may

have led to a biased sample. For example, as noted in Paper I, the source catalog for the “Ursa Major filament” study, the RC3, suffers from the “diameter-inclination effect,” which leads to a strong bias for preferentially including face-on galaxies over edge-on galaxies of the same diameter (Huizinga 1994). Finally, no attempt was made to consider the positions of the galaxies within the local large-scale structure before looking for alignments. Considering that the local mass density is critical for determining which alignment mechanism may be dominant, an attempt should be made to look for  $\vec{L}$  alignments relative to local large-scale structures. This study is an attempt to avoid some of the issues cited above and obtain a sample of galaxies with well determined  $\vec{L}$  in various environments in a supercluster using a mechanically-selected sample of galaxies.

For this study, we selected a subsample of the Minnesota Automated Plate Scanner Pisces-Perseus galaxy catalog (hereafter MAPS-PP), which is a true major-axis diameter-limited catalog built using automated, mechanical methods and does not exhibit the “diameter-inclination” effect (see Paper I). We determined the  $\vec{L}$  orientation for the galaxies in this subsample using HI observations. The sample selection criteria are outlined in Section 2. The analysis methods are discussed in Section 3. Section 4 discusses the results of the data analysis. Our interpretation of these results is provided in Section 5.

## 2. Data

The galaxy sample for this study was selected from the MAPS-PP. The MAPS-PP catalog was designed to avoid several of the pitfalls of previous attempts to measure galaxy orientations. The MAPS-PP contains  $\sim 1400$  galaxies in the Pisces-Perseus Supercluster field with (roughly) isophotal diameter  $>30''$  constructed from digitized scans of the blue and red plates of the Palomar Observatory Sky Survey (POSS I). By using a mechanical measure of the diameter, this catalog avoids the “diameter-inclination” effect seen in both the Uppsala General Catalog (Nilson 1974, hereafter UGC) and the RC3. The MAPS-PP also uses a two-dimensional, two-component fit of the galaxy light profile in order to obtain a more accurate position angle and ellipticity measurement for the component of the galaxy with most of the angular momentum (e.g. - the disk in spirals). Such a full two-dimensional fit has been shown (Byun & Freeman 1995) to be very effective at recovering the image parameters in situations where a simple ellipse fit fails (e.g. - edge-on spirals with a large bulge). More details as to the construction of the MAPS-PP are available in Paper I.

## 2.1. Selection Criteria

For this study, we selected a subsample of the MAPS-PP that could have their  $\vec{L}$  determined through HI observations and at the same time could probe the galaxy  $\vec{L}$  orientations relative to the large-scale structure of the Pisces-Perseus Supercluster (hereafter PPS). HI observations can determine which side of the major-axis is approaching us, reducing the four-fold degeneracy in the  $\vec{L}$  to two solutions. However, because of the great distance to the PPS ( $cz \approx 5500 \text{ km s}^{-1}$ ), the POSS I images don't generally have enough detail to make out spiral arm structure, so determining if we were viewing the north or south side of a galaxy would be difficult without re-imaging the galaxies. Instead, we choose to constrain the inclinations of the galaxies in our subsample to be edge-on. This means we effectively reduce the two-fold degeneracy in  $\vec{L}$  solution to a single solution and simultaneously we reduce the galaxy alignments analysis problem from a full three-dimensional problem to a much simpler one-dimensional problem. And because the PPS plane itself is viewed very close to edge-on (Giovanelli & Haynes 1988), we are simplifying the problem without losing the ability to probe the angular momentum distribution in relationship to the PPS plane. The primary requirement for including a MAPS-PP galaxy in this study was therefore an ellipticity greater than 0.66.

Other criteria for selecting a MAPS-PP galaxy for our HI program were based on observational considerations. To ensure the galaxy could be observed from Arecibo, the Declination was required to be less than  $36^\circ$ . An O (blue) major-axis diameter between  $44''$  and  $100''$  was needed so that the HI disk of the galaxy was not too small to be targeted on both sides by the Arecibo beam and not too large to be fully sampled. The galaxy was required to be within  $2.25^\circ$  of the PPS midplane (as determined in Paper I) and if the redshift was known, it needed to be between  $3500 - 7000 \text{ km s}^{-1}$  in order to increase the chances it was a true PPS member. Finally to reduce the sample size, we selected galaxies with O magnitude brighter than 17. This MAPS-PP subsample consisted of 105 galaxies.

The MAPS-PP subsample was cross-identified with the NASA/IPAC Extragalactic Database (NED) in order to obtain previous radio flux measurements and redshifts.<sup>1</sup> We also examined the field around each subsample galaxy and eliminated those in crowded fields, which led to a final MAPS-PP subsample of 96 galaxies (which will hereafter be referred to as the Arecibo sample), listed in Table 1.

---

<sup>1</sup>The NASA/IPAC Extragalactic Database (NED) is operated by the Jet Propulsion Laboratory, California Institute of Technology, under contract with the National Aeronautics and Space Administration.

## 2.2. HI Observations

We obtained 21cm line spectra with the 305m Arecibo telescope of the National Astronomy and Ionosphere Center over 14 nights between August 6 and August 20, 1998.<sup>2</sup> The new Gregorian feed was used with the narrow L band receiver using a 25 MHz bandpass centered on 1394 MHz (1024 channels). One observation was performed using a 50 MHz bandpass centered at 1400.5 MHz. The beamsize of the 305m Arecibo dish is approximately 3.3' FWHM.

For each of our Arecibo sample galaxies, we made two sets of ON-OFF observations, one 90'' to the east of the central position along the major-axis, and a corresponding observation to the west of the galaxy center. Typically, 5 minute integrations were used for each observation, although some galaxies were re-observed to allow better measurement of their weak flux and others known to be bright in HI were observed with shorter integrations.

Preliminary data reduction was performed using ANALYZ at the Arecibo facility. For each observation, the two polarizations were averaged together. For each galaxy we then archived both the sum of the east and west ( $E + W$ ) spectra and the difference (in the sense east minus west). It is the difference ( $E - W$ ) spectra that can be used to determine the spin vector, by allowing us to determine which side of the major-axis is moving toward us relative to the galaxy center. Of the 96 galaxies in the original sample, 6 were not observed, 16 were not detected in HI, 3 suffered from strong radio frequency interference (RFI), and one suffered from a distorted baseline. We therefore had a total of 70 galaxies for which there were good detections.

Subsequent data reduction was performed on the 70 galaxies for which good  $E + W$  detections existed. The spectra were Doppler corrected and the fluxes corrected for gain differences with zenith angle and changes in system temperature. A visual estimate of each galaxy's redshift was made and then radio frequency interference (RFI) within  $750 \text{ km s}^{-1}$  of the line was 'removed' from the spectra. RFI 'removal' was performed interactively and the RFI was replaced with a linear interpolation between the two endpoints of the spectra. Noise was added to the linear interpolation, using the surrounding spectral channels to determine the noise level. Both the  $E + W$  and  $E - W$  spectra were baseline corrected using a linear fit to non-HI line channels within  $500 \text{ km s}^{-1}$ .

We determined the HI line properties of the galaxy using the  $E + W$  spectra. All velocities follow the optical convention,  $v = c\Delta\lambda/\lambda_0$ , and are adjusted to be in the

---

<sup>2</sup>The National Astronomy and Ionosphere Center is operated by Cornell University under a cooperative agreement with the National Science Foundation.

heliocentric frame. The flux-weighted mean velocity,  $v_0$ , of the galaxy as well as the line flux is computed. The line width used the mean of the line widths at a threshold of 50% of the boxcar equivalent flux and at a threshold of 20% the maximum flux determined by using a outward searching algorithm (Lavezzi & Dickey 1997). The reported line width has been corrected for noise and channel width using the method outlined in Lavezzi and Dickey (1997).

### 2.3. Determination of Galaxy Spin Vector Directions and Uncertainty

The direction of the galaxy’s spin vector was determined by taking the first moment of the  $E - W$  spectra,  $\mu_{E-W}$ , where

$$\mu_{E-W} = \frac{\int_{v_{min}}^{v_{max}} f_{E+W}(v) f_{E-W}(v) (v - v_0) dv}{\int_{v_{min}}^{v_{max}} [f_{E+W}(v)]^2 dv}, \quad (1)$$

where  $v_{min}$  and  $v_{max}$  are the minimum and maximum velocity of the line respectively,  $v_0$  is the flux-weighted mean velocity of the galaxy, and  $f_{E+W}(v)$  and  $f_{E-W}(v)$  are the fluxes of the  $E + W$  and  $E - W$  spectra respectively. Negative  $\mu_{E-W}$  implies that the eastern side of the galaxy is approaching us relative to the galaxy center, meaning the galaxy’s  $\vec{L}$  points northward. Positive  $\mu_{E-W}$  implies  $\vec{L}$  points to the south.

The uncertainty in  $\mu_{E-W}$  due to bad baseline and spectral noise was measured using two variants of the normal first moment. To determine the effect of spectral noise on the first moment, we computed  $\mu_{offset}$ , where we measure the first moment of the flux outside the line by conserving  $\Delta v = (v_{max} - v_{min})$ , but offset the  $v_0$ ,  $v_{min}$ , and  $v_{max}$  in equation 1 to lie outside the line (see Figure 1). This gave us a measure of the contribution of spectral noise (presumably similar outside the HI line as inside) to the value of  $\mu$ . To determine the effect of uncertainty in the baseline fit to the first moment determination, we also computed  $\mu_{wide}$ , where we find the 1st moment about  $v_0$  of the flux outside the line. We then scaled this by  $\overline{\Delta v} / \overline{\Delta v_{outside}}$  to determine the amount of  $\mu_{E-W}$  uncertainty due to uncertainty in the baseline fit. Both  $\mu_{offset}$  and  $\mu_{wide}$  are illustrated in Figure 1.  $\mu_{offset}$  and  $\mu_{wide}$  measurements suggest that galaxies with  $|\mu_{E-W}| < 15 \text{ km s}^{-1}$  should be considered to have undetermined spin (see Figure 2).

To confirm that the  $E - W$  spectra are the result of gas being observed on both sides of the major axis, we also computed the cross-correlation,  $P_{cc}$ , of the  $E + W$  and  $E - W$  spectra,

$$P_{cc} = \frac{\int_{v_{min}}^{v_{max}} f_{E+W}(v) f_{E-W}(v) dv}{\int_{v_{min}}^{v_{max}} [f_{E+W}(v)]^2 dv}, \quad (2)$$

since we would expect that the  $E + W$  and  $E - W$  spectra would be orthogonal in those cases where the flux is from both the eastern and western positions. We have empirically found that if  $P_{cc} > 0.4$  the  $E - W$  flux was likely to be entirely from only one position and thus the spin measurement should be considered undetermined. It should be noted that this process will not eliminate observations of galaxies with an asymmetric HI distribution if there is significant flux in both the eastern and western positions. Such a asymmetric HI distribution would affect the mean velocity,  $v_0$ , and thus may affect the amplitude of  $\mu_{E-W}$ , but it should not change the sign of  $\mu_{E-W}$ , which is the observable we use later.

The final dataset had 54 galaxies with well determined spin vectors out of the 70 galaxies with good HI detections (see Table 2), 16 galaxies having been rejected from the sample due to either large  $P_{cc}$  or small  $\mu_{E-W}$ . For these galaxies, we computed

$$\theta_{\vec{L}} = \theta + 90^\circ(\mu_{E-W}/|\mu_{E-W}|), \quad (3)$$

which is the projection of  $\vec{L}$  on the plane of the sky. Since the Arecibo sample is chosen to be nearly edge-on,  $\theta_{\vec{L}}$  is essentially a complete description of  $\vec{L}$ , allowing simple one-dimensional statistical analysis to be used for what is normally a three-dimensional problem.

### 3. Data Analysis Methods

#### 3.1. The Kuiper Statistic

Identification of anisotropies in the observed  $\theta_{\vec{L}}$  and  $\theta$  distributions was initially done by using the Kuiper V statistic, which is a two-sided variant of the Kolmogorov-Smirnov (K-S) D statistic (Press *et al.* 1992). We use the Kuiper V statistic because the K-S D statistic can systematically underestimate the significance of differences between the observations and the models, especially if the differences are near the ends of the distribution (Press *et al.* 1992). For this test, we compare the cumulative distributions of a variable,  $x$  (such as  $\theta_{\vec{L}}$ ,  $\Delta\theta_{\vec{L}}$ , etc.), in the observed sample,  $S(x)$ , with that for a model of 100000 randomly-oriented galaxies,  $S_m(x)$ . The Kuiper statistic,  $V$ , is then defined as

$$V = D_+ + D_- = \max[S(x) - S_m(x)] + \max[S_m(x) - S(x)], \quad (4)$$

the sum of the absolute values of the maximum positive ( $D_+$ ) and negative ( $D_-$ ) differences between  $S(x)$  and  $S_m(x)$ .<sup>3</sup>  $V$  is essentially a measure of the difference between two

---

<sup>3</sup>Note that the normal K-S D statistic is equal to  $\max|S(x) - S_m(x)|$ . It doesn't distinguish between differences above or below the  $S_m(x)$  the curve.

distributions (see Figure 4). If the number of degrees of freedom is known a priori, a simple functional form exists for the probability,  $P(V)$ , that the two samples whose cumulative distributions differ by  $V$  were drawn from the same parent distribution (see Press *et al.* 1992, for example). Therefore, if we are comparing the distribution of  $x$  for the observed sample to that of a modeled, randomly-oriented sample, we have a way of estimating the probability that the observed sample is drawn from an isotropic distribution. In this study, we considered a distribution’s anisotropy significant if the probability,  $P(V)$ , that the Arecibo sample could have been drawn from the randomly-oriented sample was less than 5%.

In those cases where the number of degrees of freedom is not well determined a priori, we used Monte Carlo comparisons of the observations with 1000 model samples of equal size. This was necessary in order to avoid overestimating the significance of an observed anisotropy. We model a randomly oriented distribution of galaxies by taking the observed sample, randomly reassigning the observed  $P_{cc}$  and  $\mu$  values to various galaxies ( $\mu$  is determined by randomly reversing the sign of  $|\mu|$ ), and then randomly generating the major-axis position angle,  $\theta$ . This model kept the spatial distribution of the original sample and the HI observational selection effects while otherwise being a completely randomly oriented model. Comparison of the real distribution of a variable versus its distribution in the 1000 Monte-Carlo samples is used to determine the significance of an anisotropy in some of the more complicated distributions discussed in section 4.

## 4. Results and Analysis

### 4.1. Probing for Global Spin Vector Alignments

As a followup to the work done in Paper I, we initially examined some of the distributions similar in nature to the ones investigated that study. We divided the entire MAPS-PP and Arecibo Samples into 3 subsets each: the high density subset, the low density subset, and the complete sample. The high and low density subsets were created using surface density estimates,  $\Sigma$ , from the MAPS-PP catalog to compute the median surface density. The high and low density subsets include all galaxies with  $\Sigma$  greater than and less than this median value, respectively. For the MAPS-PP subsets we tested the  $\theta$ -based distributions, whereas for the Arecibo subsets, we tested the  $\theta_{\tilde{L}}$ -based distributions. Examinations of the  $\theta_{\tilde{L}}$  and  $\theta$  distributions show no significant anisotropy in any of the Arecibo or MAPS-PP subsets. Similar results were seen for distributions of  $\theta_{\tilde{L}}$  and  $\theta$  relative to other critical angles including the following:



- $\Delta\theta_{\vec{L}}(1)$  and  $\Delta\theta(1)$ : the difference of  $\theta_{\vec{L}}$  and  $\theta$ , respectively, between nearest neighbor galaxies in that sample. Note that  $\Delta\theta(1)$  is used in the Arecibo sample only to separate the significance of any  $\Delta\theta_{\vec{L}}(1)$  alignments from any  $\Delta\theta(1)$  alignments.
- $\Delta\theta_{\vec{L}}(Geo)$ : the difference of  $\theta_{\vec{L}}$  from the geodesic to the nearest neighbor galaxy.
- $\Delta\theta_{\vec{L}}(Ridge)$ : the difference of  $\theta_{\vec{L}}$  from angle of the Pisces-Perseus Supercluster ridgeline at its nearest point (as determined in Paper I).
- $\Delta\theta_{\vec{L}}(GC - X)$ : the difference of  $\theta_{\vec{L}}$  from the galaxy concentration position angle built using a percolation length of  $X$  arcminutes (galaxy concentrations groupings of galaxies identified using a 2 dimensional friends-of-friends algorithm (redshift is ignored), see Paper I for details).
- $\Delta\theta_{\vec{L}}(GCR - X)$ : the difference of  $\theta_{\vec{L}}$  from the radial line to the center of the galaxy concentration built using a percolation length of  $X$  arcminutes.

These results, shown in Table 3, support the observations in Paper I in that no simple  $\theta$  or  $\theta_{\vec{L}}$  alignments appear to be present. Examination of the  $\Delta\theta_{\vec{L}}(GC - X)$  distribution does not support the tentative anti-alignments seen in Paper I. We looked for ‘twisting’ of  $\Delta\theta_{\vec{L}}(Ridge)$  versus distance from the PPS ridgeline, and could not corroborate this signal seen in the  $\Delta\theta(Ridge)$  distribution of the MAPS-PP in Paper I. We note that the Arecibo sample is considerably smaller than the MAPS-PP, so we cannot rule out the trends seen in Paper I, but we simply cannot support them.

## 4.2. Probing for Spin Vector Domains

An initial visual inspection of the plot of the distribution of  $\theta_{\vec{L}}$  on the sky (Figure 5) appears to show some  $\theta_{\vec{L}}$  alignments. Specifically, in many cases if you pick a galaxy at random and then compare its  $\theta_{\vec{L}}$  with that of nearby galaxies, the difference is often less than  $90^\circ$ . It appeared to the authors that there was a visual impression of the PPS being divided up into “spin vector domains,” regions with preferred  $\vec{L}$  orientations. Because visual impressions are subjective, we devised tests to look for possible spin vector domains as well as looking for the alignments of the sort reported in Paper I for the galaxy major-axes.

We attempted to confirm visual impression of  $\vec{L}$  domains seen in Figure 5 by examining the orientations of several nearest neighbors, instead of just the nearest neighbor. To this end, we computed the  $\Delta\theta_{\vec{L}}(N)$  distribution, which is the summed distribution of  $\Delta\theta_{\vec{L}}$

(respectively) for the  $N$  closest galaxies within  $3^\circ$  of each galaxy. If  $\vec{L}$  domains exist, the  $\Delta\theta_{\vec{L}}(N)$  distribution should be peaked toward the lower values of  $\Delta\theta_{\vec{L}}(N)$ .

Because the  $\Delta\theta_{\vec{L}}(N)$  distribution about one galaxy is not independent of the distribution about that galaxy’s nearest neighbors, the number of degrees of freedom is uncertain *a priori*. This means that the standard function to determine the probability,  $P(V)$ , of two distributions being identical doesn’t work. Instead, we gauge  $P(V)$  by generating 1000 Monte Carlo samples and computing the Kuiper V statistic of their  $\Delta\theta_{\vec{L}}(N)$  distributions. By comparing the value of V for the observed sample with the distribution of V in the 1000 Monte Carlo samples, we have an estimate of the likelihood that a greater value of V is obtained,  $P(> V)$ . We therefore use  $P(> V)$  in leu of the  $P(V)$  used in cases where we know the number of degrees of freedom.

We examined the  $\Delta\theta_{\vec{L}}(N)$  distributions for the  $N$  closest galaxies of the Arecibo samples, for  $N$  ranging from 3 to 10. These samples show no significant anisotropy when compared to Monte Carlo generated datasets, indicating that the visual impression of  $\vec{L}$  domains is either incorrect, or the  $\vec{L}$  domains are too weakly aligned to confirm with this test.

Because in Paper I only a simple nearest neighbor test was performed, we also examined the  $\Delta\theta(N)$  distribution for the MAPS-PP samples, in order to see if  $\vec{L}$  domains might be visible in the larger MAPS-PP dataset. We found that for  $N$  ranging from 3 to 10, the  $\Delta\theta(N)$  distributions showed no evidence of significant anisotropies. This appears to indicate that it is unlikely that  $\vec{L}$  domains exist in the Pisces-Perseus Supercluster.

### 4.3. Establishing Limits on Galaxy Alignments

In order to quantify the largest anisotropic signature that could remain “hidden” from our statistical techniques, we performed a simple simulation. We generated samples drawn from random ‘sinusoidal’ distributions described by the probability distributions

$$P(\Theta)d\Theta = \left[1 + \alpha \cos\left(\Theta \frac{2\pi}{\lambda}\right)\right] d\Theta, \text{ where } \Theta \in [0, \lambda], \quad (5)$$

and

$$P(\Theta)d\Theta = \left[1 + \alpha \cos\left(\Theta \frac{2\pi}{\lambda}\right)\right] d\Theta, \text{ where } \Theta \in \left[0, \frac{\lambda}{2}\right], \quad (6)$$

where  $\alpha$  is the amplitude of the ‘sinusoidal’ component of the probability in percent. In these two distributions,  $\Theta$  represents either the expected  $\theta$  or  $\theta_{\vec{L}}$  distributions in the cases of large-scale alignments (equation 6), or the  $\Delta\theta$  and  $\Delta\theta_{\vec{L}}$  distributions in the cases of

alignments (equation 6), anti-alignments (equation 6) or both (equation 5) between nearby galaxies. Using these two distributions, we can generate samples with a predetermined amplitude,  $\alpha$ , for the alignments present and then compute the value of  $P(V)$ , the probability of the sample having been drawn from a random sample. By repeatedly doing this, we can determine the distribution of  $P(V)$  for a given  $\alpha$  and sample size.

For samples of 30, 54, 100, 615, and 1230 galaxies (the sizes of our subsets as noted in Table 3), we computed the  $P(V)$  distribution for 100 generated  $\Theta$  samples with amplitudes,  $\alpha$ , ranging from 0% to 100% in steps of two percent (see Figure 7). We then examined at which point 95% of the  $P(V)$  distribution dropped below 0.05, our criterion for calling a distribution significantly anisotropic. This gave us an estimate of the largest amplitude sinusoidal anisotropy that could have been missed, which we call  $\alpha_{95}$ .  $\alpha_{95}$  is therefore the smallest amplitude of a sinusoidal anisotropy for which there is a 95% chance of detection given the criteria of  $P(V) < 0.05$ .

For our Arecibo sample, we find that with 54 galaxies  $\alpha_{95} \approx 0.75$ , therefore we can only eliminate global spin vector alignments with sinusoidal amplitudes greater than 75%. This sample does not place very strong limits on level of any spin vector alignments present. With the 1230 galaxies in the MAPS-PP catalog, we find  $\alpha_{95} \approx 0.15$ . Therefore we can eliminate the possibility of galaxy major-axis alignments at amplitudes greater than 15%. Major-axis alignments place very weak limits on the level of spin vector alignments due to the fact that the orientation of the major-axis of the galaxy, with no additional information, only restricts the spin vector to a plane. However, if there is a spin vector alignment, it must be reflected in the major-axis distribution of the edge-on galaxies. We find that in a subsample of 729 MAPS-PP galaxies restricted to  $\epsilon > 0.50$ , there is no significant major-axis anisotropy of any sort. For a sample of 729 galaxies, we find  $\alpha_{95} \approx 0.20$ , therefore, we can confidently state that there are no spin vector alignments with sinusoidal amplitude greater than 20% (within the uncertainty due to the two-fold degeneracy in mapping major-axis position angle to spin vector).

We would like to have computed  $\alpha_{95}$  for the spin vector domain tests in order to gauge their sensitivity but it was computationally too expensive.

## 5. Conclusions

We have constructed the only catalog of well determined spin vectors for galaxies in the Pisces-Perseus Supercluster. Our study is the first radio study that explicitly looks at the spin vector distribution of galaxies in a supercluster and was optimized toward that end.

We developed a simple technique for obtaining spin vector determinations and accessing the level of uncertainty in the spin vector determinations due to both spectral noise and uncertainty in fitting the continuum. We were intentionally rather conservative in our data selection criteria, possibly rejecting several well measured spin vectors.

There are several problems currently hampering the determination of the angular momentum distribution of galaxies relative to each other and to the surrounding large-scale structure. One major problem is that we do not have a very clear understanding of the internal extinction in galaxies and its effect on the appearance of the galaxy with changing inclination. Therefore, it is very difficult to accurately determine the inclination of a galaxy based solely on its ellipticity and position angle. This also makes it more difficult to construct a proper volume-limited sample for a large-scale angular momentum study. One could obtain redshifts for all the galaxies in a diameter-limited or magnitude-limited galaxy catalog and select a volume-limited subsample, but without a clear understanding of internal extinction, we cannot correct magnitudes and diameters for inclination.

We compensated for these uncertainties of the effects of internal galaxy extinction by restricting our sample to highly edge-on galaxies. This had the added benefit of making the HI spectra of the galaxies as broad as possible, and thus making it easier to determine the  $\vec{L}$  orientation. We note that this restriction to edge-ons could make reduction of alignments relative to large-scale structure difficult, since we would be restricting analysis to galaxies with  $\vec{L}$  in the plane of the sky. However, in this study, the edge-on orientation of the Pisces-Perseus Supercluster means our sample galaxies'  $\vec{L}$  lie in the plane perpendicular to the supercluster plane, which is advantageous for reducing the complexity of the analysis. This does reduce our sensitivity to any  $\vec{L}$  alignments that lie outside the plane of the sky. For example, if galaxies'  $\vec{L}$  are preferentially oriented in a given direction within the plane of the Pisces-Perseus Supercluster (e.g. toward a cluster in the supercluster plane) rather than simply being restricted to that plane, we may not detect such an alignment in our sample, since we restrict  $\vec{L}$  of sample galaxies to the plane perpendicular to the supercluster plane. It would be interesting to perform similar observations of a “face-on” version of Pisces-Perseus, where we would then be restricting  $\vec{L}$  to the supercluster plane and possibly investigating a new class of  $\vec{L}$  alignments.

The technique we outline for obtaining spin vector measurements could be applied to quickly obtain  $\vec{L}$  measurements for many galaxies in superclusters other than Pisces-Perseus. It is also notable that this technique could be transferred to multi-fiber spectroscopy. By assigning two fibers to each galaxy, one could simultaneously determine the  $\vec{L}$  directions of many galaxies much more quickly than a comparable line slit spectrograph observations. No rotation curve information would be available, but it would allow quick collection of a

large sample of well determined galaxy  $\vec{L}$ .

Our examination of the  $\vec{L}$  distribution of galaxies in Pisces-Perseus provides no support for any form of anisotropic  $\vec{L}$  distribution. We do not provide confirmation of the possible  $\vec{L}$  alignments noted in Paper I for the major-axis distributions of Pisces-Perseus galaxies. Given the relatively small size of the Arecibo sample, rather large anisotropies in the spin vector distribution of the Arecibo sample (see Section 4.3) could remain undetected with our technique. We do note that by using a sample of 729 nearly edge-on galaxies from the original MAPS-PP catalog, we feel we can restrict the sinusoidal amplitude of any spin vector anisotropy present to be less than approximately 20% the background ‘random’ distribution, at least in the plane perpendicular to the Pisces-Perseus supercluster ridge.

It is unclear at what level galaxy  $\vec{L}$  alignments might be expected as no recent simulations have been designed with the goal of estimating galaxy alignments. We expect that if galaxy alignments are produced by large-scale structure formation, the alignments would be strongest in areas of low density, where the relative scarcity of subsequent galaxy-galaxy interactions suggests the initial  $\vec{L}$  distribution would be better preserved. However, as noted in the introduction, galaxy alignments can arise from a variety of evolutionary processes, in both high and low density environments. It would be interesting if in modern computer simulations of galaxy evolution, the angular momentum of the resulting galaxies was investigated for  $\vec{L}$  alignments and predictions as to the amplitude (and type) of any anisotropies in the  $\vec{L}$  distribution were made.

As we showed in Section 4.3, sample sizes need to be large (on the order of at least 500 galaxies) in order to unambiguously detect weak alignments. There are two paths toward increasing the sample size. We could examine a denser cluster with a greater number of targets satisfying our edge-on criteria such as the Coma cluster. It would be interesting to investigate the possibility of tidally induced galaxy alignments in denser environments as predicted by Ciotti and Dutta (1994) and Ciotti and Giampieri (1998). The only previous study looking for galaxy alignments in Coma was plagued by stretched imaging (Djorgovski 1987), so alignment results for this cluster are still unclear. Our other option for increasing sample size is to develop a better understanding of the internal extinction in galaxies so that we could use galaxies of all inclinations. The first author is currently investigating using image parameters of a large number of galaxies obtained using the APS database in order to better determine the internal extinction properties of galaxies.

We would like to thank telescope operators Miguel Boggiano, Willie Portalatin, Pedro Torres, and Norberto Despiau for their good humor and help with observing (And especially Norberto for his “lucky coffee”). JEC would like to thank Chris Salter, Tapasi Ghosh, Jo Ann Etter, and Phil Perillat for helping make his first radio observing experience excellent,

both professionally and personally. Travel was sponsored by the National Astronomy and Ionosphere Center (NAIC) and the University of Minnesota Graduate School.

This research has made use of the APS Catalog of the POSS I, which is supported by the National Aeronautics and Space Administration and the University of Minnesota. The APS databases can be accessed at <http://aps.umn.edu/> on the World Wide Web. Some data reduction was performed at the Laboratory for Computational Science and Engineering (LCSE) at the University of Minnesota. Information about the LCSE can be found online at <http://www.lcse.umn.edu/>.

Table 1. The Arecibo Sample (A subset of 96 MAPS-PP galaxies)

APS ID	Common Name <sup>a</sup>	$\alpha$ (B1950)	$\delta$ (B1950)	$m_O$ <sup>b</sup>	$O - E$ <sup>b</sup>	$a_O$ <sup>b</sup>	$R_{ridge}$ <sup>c</sup> ( $^{\circ}$ )	$\Sigma$ <sup>c</sup>
O_778_873376	UGC 11993	22:18:25.5	34:58:14.8	15.67	1.49	61.7	0.89	5.60
O_778_731211	22208+3548	22:20:49.5	35:48:04.8	14.66	1.42	52.0	0.25	25.35
O_778_700353	22233+3556	22:23:19.2	35:55:31.0	15.32	1.52	57.4	0.58	10.40
O_778_847676	None	22:24:45.4	35:10:40.3	15.41	1.39	44.0	0.27	11.23
O_778_849054	None	22:25:53.3	35:04:31.8	15.39	1.66	46.7	0.12	9.07
O_778_1040599	NGC 7320B	22:35:10.3	33:39:46.9	15.54	1.47	49.2	0.34	7.17
O_778_923367	None	22:39:36.3	34:39:30.7	14.03	1.39	94.8	1.12	6.39
O_778_755586	None	22:41:32.8	35:38:55.2	15.39	1.52	52.1	2.19	3.20
O_1184_28270	None	22:50:24.2	33:07:53.6	16.26	1.64	44.3	0.86	3.11
O_1184_66567	22508+3230	22:50:47.0	32:29:50.0	14.99	1.44	49.5	0.32	11.28
O_1184_128370	UGC 12231	22:51:11.0	31:21:11.7	14.84	-0.35	62.4	0.84	10.07
O_1184_81567	None	22:55:40.5	32:11:55.6	15.90	1.34	49.2	0.12	6.26
O_1184_196807	UGC 12320	22:59:40.4	30:29:42.0	15.83	1.45	66.8	1.50	6.00
O_1184_121956	UGC 12362	23:03:51.4	31:36:49.0	14.44	1.00	67.4	0.17	2.27
O_1184_275037	MCG +05-54-039	23:07:04.4	29:12:43.0	15.38	1.16	53.0	1.43	2.35
O_1184_313727	UGC 12427	23:10:57.6	28:40:55.9	14.94	0.19	49.4	0.97	5.94
O_1184_347214	None	23:12:38.9	28:00:36.0	15.60	0.46	52.7	0.99	6.24
O_1184_189398	UGC 12458	23:12:43.0	30:40:27.0	16.22	1.51	59.9	0.52	6.82
O_843_144830	None	23:18:38.9	25:22:01.9	15.86	1.50	44.0	2.07	4.80
O_843_65466	None	23:18:59.9	26:12:15.6	15.95	0.96	44.9	1.31	4.95
O_914_404205	UGC 12557	23:20:01.1	28:54:24.1	14.72	1.49	75.0	0.86	5.05
O_914_406137	None	23:23:49.0	28:58:48.0	16.70	1.46	44.8	1.60	5.66
O_914_344933	UGC 12625	23:26:38.5	29:29:58.3	14.73	1.57	84.2	1.72	4.36
O_914_409641	UGC 12644	23:28:58.8	28:54:47.7	14.86	0.56	59.1	0.95	3.69
O_914_371708	None	23:32:07.5	29:26:30.5	16.45	1.45	48.7	0.89	3.28
O_914_413061	None	23:32:17.4	29:02:11.2	16.07	1.47	45.5	0.59	3.05
O_914_511814	None	23:33:55.7	27:39:32.0	16.07	1.24	55.7	0.72	3.32
O_914_416774	UGC 12730	23:38:03.3	28:54:39.3	14.29	1.56	98.6	0.32	2.84
O_914_286281	UGC 12741	23:39:25.1	30:18:15.5	14.54	0.94	57.3	0.74	1.49
O_914_286479	None	23:39:59.4	30:19:12.6	15.63	0.68	44.0	0.72	1.50
O_914_514191	None	23:40:00.1	27:46:03.4	16.26	1.17	52.8	1.53	6.24
O_914_437214	CGCG 498-006	23:42:35.0	28:47:11.1	15.55	1.38	46.1	0.93	4.75
O_1257_181710	MCG +05-01-003	23:52:48.7	30:06:24.8	15.11	1.51	54.2	0.27	3.38
O_1257_106449	UGC 12845	23:53:09.1	31:37:15.8	15.11	1.99	52.4	1.25	2.20
O_1257_149828	UGC 12864	23:54:50.8	30:42:49.4	14.49	1.11	85.0	0.34	3.85
O_1257_140283	NGC 7799	23:56:46.8	31:00:22.1	15.96	1.19	66.9	0.64	2.90
O_1257_307025	UGC 124	00:10:48.1	28:05:27.8	15.45	1.85	55.1	2.12	5.95
O_1257_224112	UGC 147	00:13:07.5	29:23:21.2	15.39	1.83	45.6	0.79	7.56
O_1257_212633	00139+2939	00:13:52.2	29:38:45.5	15.37	0.78	67.6	0.53	18.31
O_1244_265500	UGC 238	00:22:25.5	31:03:58.5	13.70	1.15	99.0	0.99	3.82
O_1244_376417	00254+3029	00:25:21.3	30:29:18.9	15.20	1.34	55.9	0.48	5.08
O_1244_340721	UGC 279	00:25:36.7	30:31:37.5	13.90	1.09	92.3	0.51	4.61
O_1244_270335	00267+3106	00:26:45.2	31:06:17.2	15.57	1.07	83.8	1.12	6.73
O_1244_679996	UGC 310	00:28:39.0	28:42:58.5	14.84	0.62	68.2	1.23	2.29
O_1244_578706	None	00:29:14.4	29:25:41.8	15.88	0.74	45.7	0.54	3.48
O_1244_241809	00313+3110	00:31:15.4	31:10:30.6	15.40	0.00	55.4	1.30	4.67
O_1244_767827	UGC 345	00:32:09.7	28:08:02.5	15.22	0.09	76.1	1.75	1.76
O_1244_185805	00333+3136	00:33:15.9	31:35:41.4	14.23	1.24	68.0	1.75	3.54
O_1244_655424	00347+2853	00:34:41.6	28:52:27.1	14.85	0.84	98.4	0.95	7.96
O_1244_554203	UGC 412	00:36:49.5	29:29:16.8	15.25	1.29	55.9	0.34	10.90

Table 1—Continued

APS ID	Common Name <sup>a</sup>	$\alpha$ (B1950)	$\delta$ (B1950)	$m_O$ <sup>b</sup>	$O - E$ <sup>b</sup>	$a_O$ <sup>b</sup>	$R_{ridge}$ <sup>c</sup> ( $^{\circ}$ )	$\Sigma$ <sup>c</sup>
O_1244_595079	UGC 449	00:39:41.7	29:25:26.2	14.96	0.93	63.5	0.40	7.98
O_1244_521380	None	00:40:48.3	29:46:45.6	15.32	0.75	51.2	0.04	12.24
O_1244_442897	None	00:41:53.2	30:04:51.5	16.59	0.50	47.1	0.42	11.42
O_1244_484644	UGC 478	00:43:44.5	29:57:54.9	14.45	1.13	80.4	0.17	13.26
O_601_2598615	UGC 501	00:46:21.1	27:56:44.1	15.47	1.55	91.9	1.95	2.21
O_601_927741	UGC 511	00:47:27.3	31:27:32.8	15.46	0.96	69.8	1.47	5.16
O_601_2448395	CGCG 501-024	00:48:09.5	28:25:40.3	15.69	1.19	44.6	1.50	4.85
O_601_1985337	UGC 525	00:48:52.4	29:26:42.9	15.69	1.42	73.9	0.64	4.96
O_601_1986315	00494+2924	00:49:30.1	29:24:19.4	14.42	1.67	60.4	0.66	6.53
O_601_2601958	None	00:50:49.0	28:00:21.8	16.80	1.60	53.5	2.08	3.56
O_601_1152906	UGC 557	00:52:03.8	31:05:40.0	14.56	0.73	59.5	0.76	20.54
O_601_2454111	UGC 554	00:52:04.6	28:26:44.9	15.22	1.79	50.9	1.71	5.65
O_601_2363374	00521+2835	00:52:06.5	28:35:46.1	14.78	1.79	58.7	1.57	4.48
O_601_1044227	UGC 565	00:52:38.6	31:24:14.1	15.13	0.98	48.1	0.92	13.23
O_601_1267760	CGCG 501-048	00:53:26.0	30:48:15.4	15.38	1.21	55.5	0.47	9.02
O_601_1050939	UGC 598	00:55:06.2	31:12:52.1	14.19	1.44	71.3	0.49	6.20
O_601_1498038	UGC 624	00:57:52.7	30:23:58.1	13.00	0.96	99.9	0.60	6.63
O_601_1063679	UGC 633	00:58:37.0	31:14:23.6	14.16	0.95	90.7	0.01	6.20
O_601_863271	None	01:00:55.7	31:46:46.0	15.29	1.04	60.7	0.15	8.98
O_601_1294945	01011+3056	01:01:04.3	30:55:47.2	15.71	1.11	57.4	0.61	4.65
O_601_978154	UGC 669	01:02:34.0	31:24:52.0	15.19	1.32	72.1	0.39	6.37
O_601_1197694	UGC 673	01:03:24.6	31:08:18.2	15.15	0.81	57.1	0.72	4.65
O_601_657010	UGC 679	01:04:17.9	32:07:21.1	16.17	0.63	51.3	0.10	22.35
O_601_992015	CGCG 501-092	01:05:17.4	31:24:29.8	15.25	1.34	45.1	0.80	9.63
O_601_175820	A82-91	01:05:18.4	33:11:11.4	14.49	1.25	57.8	0.82	17.03
O_601_264028	NGC 407	01:07:49.8	32:51:38.8	14.09	1.44	96.5	0.34	18.31
O_601_359427	None	01:07:57.9	32:45:57.2	16.27	0.63	47.3	0.25	19.90
O_406_436424	01104+3443	01:10:24.4	34:42:01.4	16.52	0.66	49.0	1.94	2.14
O_406_502375	UGC 809	01:13:04.0	33:32:50.3	14.84	0.74	74.2	0.68	2.66
O_1189_285025	None	01:19:39.9	33:46:42.9	15.99	0.83	45.8	0.69	8.12
O_1189_293769	NGC 512	01:21:10.7	33:38:47.5	13.74	1.05	69.5	0.49	6.95
O_1189_251296	01287+3432	01:28:43.2	34:31:32.6	14.81	0.55	56.1	0.76	3.02
O_1189_224928	NGC 634	01:35:25.4	35:06:38.8	13.70	1.13	84.6	0.57	3.98
O_1189_244311	UGC 1166	01:35:42.0	34:44:18.4	14.17	1.23	71.1	0.39	3.38
O_1189_234487	01366+3455	01:36:39.7	34:54:18.6	15.20	0.61	45.6	0.25	3.32
O_1189_216659	NGC 653	01:39:31.7	35:23:12.3	14.17	1.42	83.3	0.36	2.96
O_1189_199608	01446+3547	01:44:34.6	35:47:04.8	14.76	1.08	44.8	0.39	5.38
O_1225_610652	None	01:45:28.6	33:35:47.0	16.99	0.52	48.1	1.81	2.49
O_1225_389102	UGC 1307	01:47:51.9	35:41:06.0	14.32	1.34	76.9	0.26	18.09
O_1225_412197	UGC 1339	01:49:28.8	35:36:36.5	14.39	1.55	48.8	0.29	34.59
O_1225_369028	NGC 714	01:50:33.0	35:58:31.7	14.06	1.62	77.5	0.20	42.61
O_1225_369332	UGC 1363	01:50:58.4	35:59:02.1	14.71	1.49	70.0	0.29	47.93
O_1225_394977	01561+3549	01:56:09.1	35:49:14.2	14.93	1.48	79.2	0.12	9.32
O_1225_484388	UGC 1569	02:01:55.5	34:54:35.3	15.47	1.46	47.3	0.53	2.50
O_1225_531870	02023+3434	02:02:19.7	34:33:02.9	15.01	1.15	51.8	0.76	2.67
O_1225_606718	02087+3349	02:08:40.7	33:48:35.6	14.64	1.13	63.9	1.58	2.54

<sup>a</sup>The common name of the object was determined via cross-identification of APS position with the NASA/IPAC Extragalactic Database (NED).

<sup>b</sup>The O bandpass magnitude ( $m_O$ ),  $O - E$  color, and O bandpass major-axis diameter ( $a_O$ ) were all obtained from the APS catalog. The  $m_O$  and  $O - E$  are zeropointed on a plate-by-plate basis as outlined in Cabanela & Aldering (1998).

<sup>c</sup>The distance from the Pisces-Perseus ridgeline ( $R_{ridge}$ ) and local surface density ( $\Sigma$ ) are from Cabanela & Aldering (1998).  $\Sigma$  is in units of galaxies/ $\square^{\circ}$ .



Table 2. The Arecibo Observations

APS ID	Date <sup>a</sup>	$V_{Sun}$ (km s <sup>-1</sup> )	$\Delta V$	$F_{obs}$ (Jy-km s <sup>-1</sup> )	Spin <sup>b</sup>	$\mu_{E-W}$ (km s <sup>-1</sup> )	$P_{cc}$	Comments
O_778_873376	11	5604	334	1.03(0.08)	N	-19.7	-0.203	
O_778_731211	08	—	—	—	U	—	—	Non-detection
O_778_700353	18	—	—	—	U	—	—	Non-detection
O_778_847676	16	—	—	—	U	—	—	Non-detection
O_778_849054	13	—	—	—	U	—	—	Non-detection
O_778_1040599	07	6379	328	1.12(0.08)	U	+14.7	-0.151	
O_778_923367	14	6576	547	2.85(0.16)	U	-11.4	+0.389	
O_778_755586	12	6661	269	1.23(0.10)	U	-8.5	-0.057	
O_1184_28270	12+17	6705	443	1.30(0.10)	S	+38.7	+0.121	
O_1184_66567	13	6791	267	0.85(0.09)	U	-6.1	+0.274	
O_1184_128370	06	3869	200	4.55(0.06)	U	-12.3	-0.023	
O_1184_81567	09	6588	283	1.50(0.07)	S	+21.8	+0.061	
O_1184_196807	06	6597	342	3.10(0.09)	S	+27.6	-0.068	
O_1184_121956	07	6436	358	9.36(0.10)	S	+41.3	-0.163	
O_1184_275037	06	3691	275	5.25(0.09)	N	-28.7	-0.030	
O_1184_313727	06	3674	224	7.24(0.08)	U	+12.4	-0.054	
O_1184_347214	14	5836	235	2.34(0.07)	U	+7.5	-0.061	
O_1184_189398	09	6838	406	1.58(0.10)	S	+25.0	+0.143	
O_843_144830	15	—	—	—	U	—	—	Non-detection
O_843_65466	16	5879	235	3.24(0.09)	U	+8.8	-0.220	
O_914_404205	07	5903	555	5.24(0.10)	N	-74.2	-0.271	
O_914_406137	13+17	5534	187	0.28(0.09)	U	+9.0	+0.300	
O_914_344933	12	5225	435	1.95(0.09)	S	+29.8	-0.210	
O_914_409641	11	5466	213	4.38(0.08)	U	+12.7	+0.001	
O_914_371708	16	—	—	—	U	—	—	Non-detection
O_914_413061	15	—	—	—	U	—	—	Non-detection
O_914_511814	20	8802	372	4.56(0.09)	S	+24.4	+0.068	50 MHz bandpass
O_914_416774	14	5191	507	3.87(0.10)	N	-42.9	+0.079	
O_914_286281	14	5208	395	6.34(0.09)	N	-36.9	-0.047	
O_914_286479	17	5057	224	1.82(0.09)	U	-11.6	-0.148	
O_914_514191	15	7134	261	3.10(0.07)	U	-13.3	+0.049	
O_914_437214	15	6895	318	1.43(0.08)	N	-20.7	-0.162	
O_1257_181710	16	5111	272	1.34(0.08)	U	+2.5	+0.214	
O_1257_106449	07	4844	245	11.67(0.06)	S	+36.4	-0.014	
O_1257_149828	12	4647	302	12.82(0.17)	N	-44.9	+0.072	
O_1257_140283	13	4970	245	5.07(0.07)	S	+20.6	+0.029	
O_1257_307025	17	—	—	—	U	—	—	Non-detection
O_1257_224112	18	—	—	—	U	—	—	Non-detection
O_1257_212633	13	4835	245	4.47(0.09)	N	-24.2	-0.001	
O_1244_265500	15	6765	411	8.75(0.12)	N	-44.2	+0.051	
O_1244_376417	15	6287	390	3.90(0.09)	U	+14.4	+0.367	
O_1244_340721	11	6269	446	10.75(0.10)	N	-46.2	-0.234	
O_1244_270335	14	6296	275	1.99(0.09)	N	-24.5	-0.058	
O_1244_679996	06	4635	179	3.15(0.14)	U	+8.9	+0.093	
O_1244_578706	17	6966	288	3.08(0.10)	U	-4.3	-0.404	
O_1244_241809	12	4593	138	5.55(0.10)	U	+11.4	+0.164	
O_1244_767827	06	4148	200	4.71(0.09)	S	+18.8	-0.015	
O_1244_185805	18	6292	419	2.05(0.10)	N	-21.7	+0.069	
O_1244_655424	14	5238	342	4.31(0.08)	N	-51.8	+0.149	
O_1244_554203	16	—	—	—	U	—	—	Non-detection
O_1244_595079	13	5249	248	5.04(0.06)	N	-30.4	+0.037	

Table 2—Continued

APS ID	Date <sup>a</sup>	$V_{Sun}$ (km s <sup>-1</sup> )	$\Delta V$	$F_{obs}$ (Jy-km s <sup>-1</sup> )	Spin <sup>b</sup>	$\mu_{E-W}$ (km s <sup>-1</sup> )	$P_{cc}$	Comments
O_1244_521380	20	4891	283	1.43(0.08)	U	-10.5	+0.181	
O_1244_442897	20	—	—	—	U	—	—	Strong RFI
O_1244_484644	18	4901	459	1.34(0.09)	N	-38.6	+0.220	
O_601_2598615	06	5059	382	4.71(0.19)	N	-52.7	-0.049	
O_601_927741	13	4575	323	3.60(0.08)	N	-28.7	-0.023	
O_601_2448395	17	4972	219	1.69(0.08)	U	-6.2	+0.907	
O_601_1985337	07	4892	227	2.97(0.07)	N	-17.8	-0.346	
O_601_1986315	18	—	—	—	U	—	—	Non-detection
O_601_2601958	None	—	—	—	U	—	—	
O_601_1152906	11	6267	446	10.77(0.10)	N	-46.2	-0.235	
O_601_2454111	None	—	—	—	U	—	—	
O_601_2363374	18	—	—	—	U	—	—	Baseline distorted
O_601_1044227	17	5635	232	1.13(0.09)	U	+18.9	+1.021	
O_601_1267760	18	4623	318	2.08(0.10)	N	-18.7	-0.071	
O_601_1050939	18	5087	146	1.42(0.07)	N	-27.4	+0.100	
O_601_1498038	12	4758	523	9.16(0.12)	N	-73.6	-0.213	
O_601_1063679	14	5535	416	7.15(0.10)	N	-42.8	+0.047	
O_601_863271	None	—	—	—	U	—	—	
O_601_1294945	16	6218	267	2.85(0.08)	N	-15.8	+0.039	
O_601_978154	20	5823	347	1.15(0.13)	U	+9.7	+0.592	
O_601_1197694	16	6213	277	3.72(0.08)	U	+13.2	+0.271	
O_601_657010	16	5069	219	2.51(0.09)	S	+18.6	+0.135	
O_601_992015	None	—	—	—	U	—	—	
O_601_175820	20	—	—	—	U	—	—	Non-detection
O_601_264028	None	—	—	—	U	—	—	
O_601_359427	20	4643	267	1.22(0.09)	U	+3.4	+0.262	
O_406_436424	20	4708	221	1.84(0.08)	S	+17.8	+0.080	
O_406_502375	16	4160	299	3.45(0.10)	U	-54.1	+0.958	
O_1189_285025	17	4851	277	1.00(0.11)	U	+0.5	+0.090	
O_1189_293769	06	4839	534	5.36(0.10)	N	-70.2	-0.008	
O_1189_251296	12	4127	213	3.28(0.07)	U	+8.9	+0.104	
O_1189_224928	13	4884	497	6.83(0.10)	S	+74.1	-0.032	
O_1189_244311	14	—	—	—	U	—	—	Strong RFI
O_1189_234487	15	5126	176	1.71(0.08)	U	-6.4	+0.164	
O_1189_216659	16	—	—	—	U	—	—	Strong RFI
O_1189_199608	17	4786	272	1.11(0.08)	N	-19.7	+0.376	
O_1225_610652	09	5728	221	1.11(0.07)	U	-12.0	-0.104	
O_1225_389102	18	—	—	—	U	—	—	Non-detection
O_1225_412197	18	—	—	—	U	—	—	Non-detection
O_1225_369028	None	—	—	—	U	—	—	
O_1225_369332	20	—	—	—	U	—	—	Non-detection
O_1225_394977	12	5406	366	1.75(0.08)	S	+34.6	+0.099	
O_1225_484388	13	—	—	—	U	—	—	Non-detection
O_1225_531870	10	4334	288	1.14(0.09)	U	+13.2	-0.211	
O_1225_606718	08	6128	435	3.33(0.10)	N	-39.1	+0.326	

<sup>a</sup>Observation date is the day of the month of August 1998. All Dates are UTC.

<sup>b</sup>There are three possible values for the spin direction, “N” for north, “S” for South, and “U” for Undetermined. The spin direction is determined from the values of  $\mu_{E-W}$  and  $P_{cc}$ .

Table 3. Arecibo  $\vec{L}$  Anisotropy Probabilities,  $P(V)$

Distribution	Arecibo Sample			MAPS-PP Catalog		
	all	hi dens	lo dens	all	hi dens	lo dens
$N_{gal}$	54	23	30	1230	616	615
$\theta_{\vec{L}}$	0.220	0.061	0.064	—	—	—
$\theta$	0.449	0.448	0.807	0.388	0.270	0.341
$\Delta\theta_{\vec{L}}(1)$	0.096	0.462	0.120	—	—	—
$\Delta\theta(1)$	0.121	0.119	0.361	0.667	0.197	0.352
$\Delta\theta(Geo)$	—	—	—	0.606	0.730	0.680
$\Delta\theta_{\vec{L}}(Geo)$	0.384	0.894	0.374	—	—	—
$\Delta\theta(Ridge)$	—	—	—	0.799	0.126	0.900
$\Delta\theta_{\vec{L}}(Ridge)$	0.257	0.142	0.113	—	—	—

“ $\Delta\theta_{\vec{L}}/\Delta\theta$ ” represents  $\Delta\theta_{\vec{L}}$  for Arecibo Sample and  $\Delta\theta$  for MAPS-PP Catalog,  
“(N)” below indicates the number of galaxies in this distribution.

$\Delta\theta_{\vec{L}}/\Delta\theta(GC - 10)$	— (000)	— (000)	— (000)	0.651 (013)	0.651 (013)	— (000)
$\Delta\theta_{\vec{L}}/\Delta\theta(GC - 15)$	0.279 (001)	0.279 (001)	— (000)	0.700 (093)	0.700 (093)	— (000)
$\Delta\theta_{\vec{L}}/\Delta\theta(GC - 20)$	0.699 (009)	0.884 (008)	0.279 (001)	0.823 (224)	0.846 (220)	0.731 (004)
$\Delta\theta_{\vec{L}}/\Delta\theta(GC - 25)$	0.489 (018)	0.954 (014)	0.108 (003)	0.113 (431)	0.062 (389)	0.797 (043)
$\Delta\theta_{\vec{L}}/\Delta\theta(GC - 30)$	0.086 (030)	0.410 (021)	0.252 (008)	0.774 (581)	0.727 (455)	0.596 (127)
$\Delta\theta_{\vec{L}}/\Delta\theta(GC - 35)$	0.046 (042)	0.065 (023)	0.160 (018)	0.590 (722)	0.881 (497)	0.639 (226)
$\Delta\theta_{\vec{L}}/\Delta\theta(GC - 40)$	0.124 (048)	0.244 (023)	0.624 (024)	0.095 (817)	0.113 (508)	0.946 (310)
$\Delta\theta_{\vec{L}}/\Delta\theta(GC - 45)$	0.214 (052)	0.016 (023)	0.815 (028)	0.307 (902)	0.380 (509)	0.692 (394)
$\Delta\theta_{\vec{L}}/\Delta\theta(GC - 50)$	0.494 (052)	0.106 (023)	0.917 (028)	0.616 (948)	0.742 (509)	0.905 (440)
$\Delta\theta_{\vec{L}}/\Delta\theta(GCR - 10)$	— (000)	— (000)	— (000)	0.858 (013)	0.858 (013)	— (000)
$\Delta\theta_{\vec{L}}/\Delta\theta(GCR - 15)$	0.279 (001)	0.279 (001)	— (000)	0.839 (093)	0.839 (093)	— (000)
$\Delta\theta_{\vec{L}}/\Delta\theta(GCR - 20)$	0.931 (009)	0.683 (008)	0.279 (001)	0.741 (224)	0.720 (220)	0.232 (004)
$\Delta\theta_{\vec{L}}/\Delta\theta(GCR - 25)$	0.764 (018)	0.365 (014)	0.850 (003)	0.779 (431)	0.665 (389)	0.862 (043)
$\Delta\theta_{\vec{L}}/\Delta\theta(GCR - 30)$	0.767 (030)	0.523 (021)	0.871 (008)	0.346 (581)	0.605 (455)	0.765 (127)
$\Delta\theta_{\vec{L}}/\Delta\theta(GCR - 35)$	0.359 (042)	0.473 (023)	0.707 (018)	0.040 (722)	0.247 (497)	0.546 (226)
$\Delta\theta_{\vec{L}}/\Delta\theta(GCR - 40)$	0.917 (048)	0.711 (023)	0.475 (024)	0.670 (817)	0.264 (508)	0.271 (310)
$\Delta\theta_{\vec{L}}/\Delta\theta(GCR - 45)$	0.281 (052)	0.253 (023)	0.428 (028)	0.457 (902)	0.849 (509)	0.127 (394)
$\Delta\theta_{\vec{L}}/\Delta\theta(GCR - 50)$	0.148 (052)	0.568 (023)	0.039 (028)	0.274 (948)	0.196 (509)	0.973 (440)

## REFERENCES

- Binggeli, B. 1982, A&A, **107**, 338
- Byun, Y.I. and Freeman, K.C. 1995, ApJ, **448**, 563
- Cabanela, J.E. and Aldering, G.L. 1998, AJ, **106**, 1094 (Paper I)
- Ciotti, L. and Dutta, S.N. 1994, MNRAS, **270**, 390
- Ciotti, L. and Giampieri, G. 1998, *astro-ph/9801261*
- Colberg, J.M., White, S.D.M., Jenkins, A., and Pearce, F.R. 1998, *astro-ph/9711040*
- de Vaucouleurs, G., de Vaucouleurs, A., Corwin, H. G. Jr., Buta, R. J., Paturel, G., Fouqué, P. 1991, *Third Reference Catalogue of Bright Galaxies* (New York, Springer-Verlag) (RC3)
- Doroshkevich, A. and Shandarin, S. 1978, MNRAS, **184**, 643
- Djorgovski, S. 1987, in *Nearly Normal Galaxies*, ed. Faber, S.M. (New York, Springer-Verlag), 227
- Flin, P. 1988, MNRAS, **235**, 857
- Giovanelli, R. and Haynes, M.P. 1988, in *Large-Scale Structures of the Universe*, eds. Audouze, J., Pelletan, M., & Szalay, A. (Dordrecht, Kluwer Academic Publishers), 113
- Han, C., Gould, A., and Sackett, P.D. 1995, ApJ, **445**, 46
- Helou, G. and Salpeter, E. 1982, ApJ, **252**, 75
- Helou, G. 1984, ApJ, **284**, 471
- Hoffman, G.L., Lewis, B.M., Helou, G., Salpeter, E.E., and Williams, H.L. 1989, ApJS, **69**, 95
- Huizinga, J. E. 1994, Ph.D. Thesis, Groningen
- Kashikawa, N. and Okamura, S. 1992, PASJ, **44**, 493
- Lavezzi, T.E. and Dickey, J.M. 1997, AJ, **114**, 2437
- Nilson, P. 1974, Uppsala Astron. Obs. Annals, No. 6 (UGC)

Press, W.H., Teukolsky, S.A., Vetterlin, W.T., and Flannery, B.P. 1992, *Numerical Recipes in C (Second Edition)* (New York, Cambridge University Press)

Sofue, Y. 1992, PASJ, **44**, L1

West, M.J. 1994, MNRAS, **268**, 79

White, S.D.M. 1984, ApJ, **286**, 38

Zel'dovich, Y.B. 1970, A&A, **5**, 84

Fig. 1.— This plot shows the ranges of velocity over which  $\mu_{E-W}$ ,  $\mu_{offset}$ , and  $\mu_{wide}$  are determined, in this case for the spectrum of UGC 12231.

Fig. 2.— The plot on the left shows the distribution of  $\mu_{E-W}$  values for the 70 Arecibo sample galaxies detected in HI. Negative  $\mu_{E-W}$  means the galaxy’s  $\vec{L}$  points northward. The right plot shows the distribution of  $\mu_{offset}$  (hatched) and  $\mu_{wide}$  (clear), both of which are have a FWHM of roughly  $15 \text{ km s}^{-1}$ .

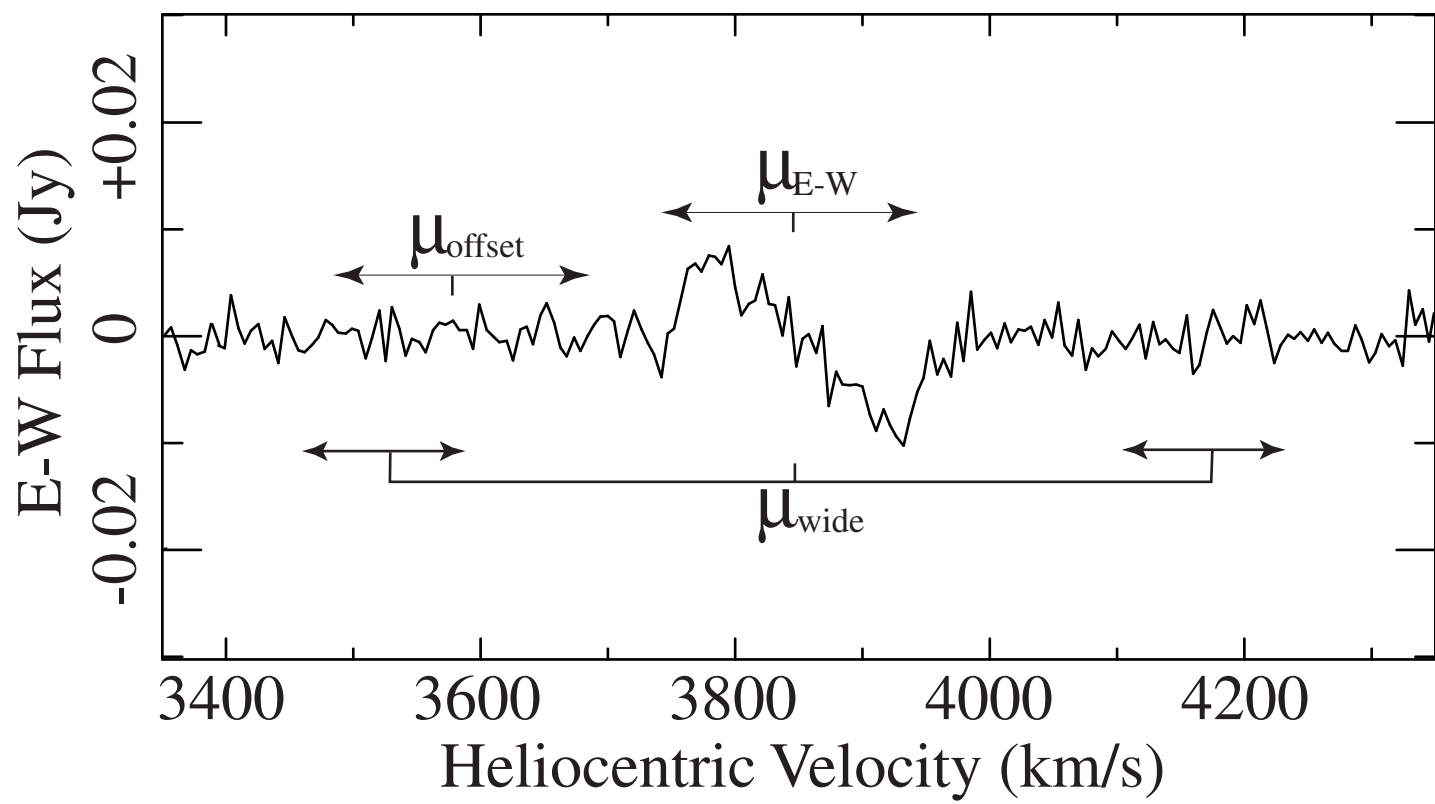
Fig. 3.— The reduced spectra for the Arecibo sample in units of Jy versus  $\text{km s}^{-1}$ . The top spectrum in each pair is  $f_{E+W}(v)$ , the bottom spectrum is  $f_{E-W}(v)$  shifted by  $-0.02 \text{ Jy}$ . Each spectrum is  $1500 \text{ km s}^{-1}$  wide and centered on the systemic heliocentric velocity of the galaxy. Spectra are baseline corrected. Gaps indicate where RFI was identified.

Fig. 4.— This diagram illustrates how the Kuiper V statistic is determined for a given cumulative distribution. The dashed line is the cumulative distribution,  $S(x)$ , of  $\Delta\theta_{\vec{L}}(1)$  for the Arecibo sample. The solid line is the modeled, isotropic distribution,  $S_m(x)$ . The maximum positive ( $D_+$ ) and negative ( $D_-$ ) differences between  $S(x)$  and  $S_m(x)$  are shown for this sample. The Kuiper V statistic is the sum of  $D_+$  and  $D_-$  whereas the K–S D statistic is  $D_+$  (because  $|D_+| > |D_-|$  in this case). It has been previously established that V is a more robust measure than D of the difference between two distributions and thus we choose to use V to measure the anisotropy of our data (see Press *et al.* 1992, for example).

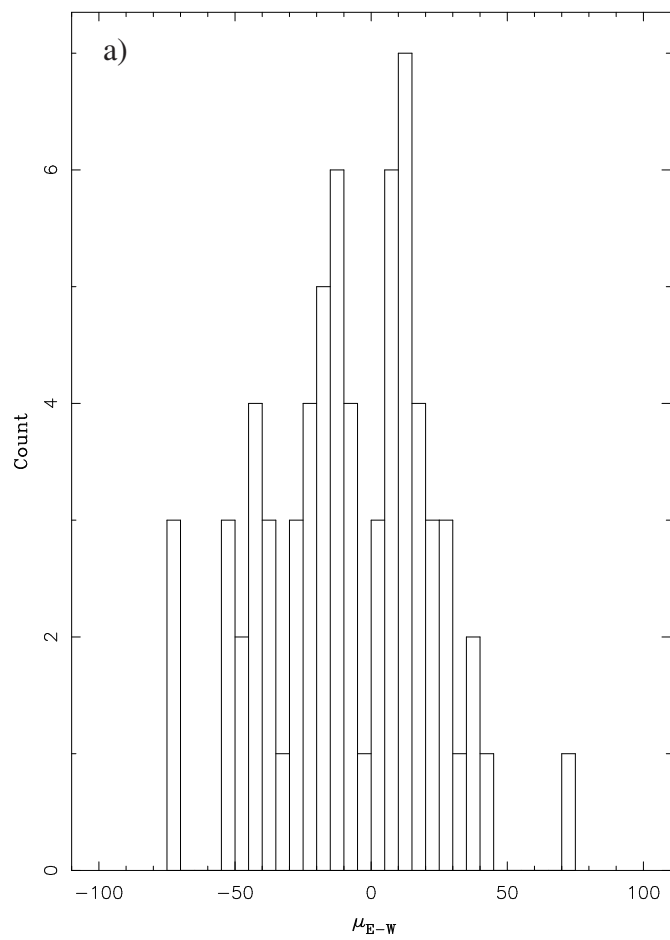
Fig. 5.— This map shows the distribution of the entire Arecibo subsample on the sky, with varying symbols depending on the value of  $\theta_{\vec{L}}$ . If  $\theta_{\vec{L}}$  is well-determined, an arrow shows its direction, if  $\theta_{\vec{L}}$  is not-well determined, but the galaxy was detected in HI, a line shows the direction of  $\theta_{\vec{L}}$ , but not the sign. A circle marks those galaxies that were undetected in HI.

Fig. 6.— This map shows the major-axis position angle distribution of MAPS-PP O sample of 1230 galaxies on the sky. Note that apparent alignments are visible to the eye.

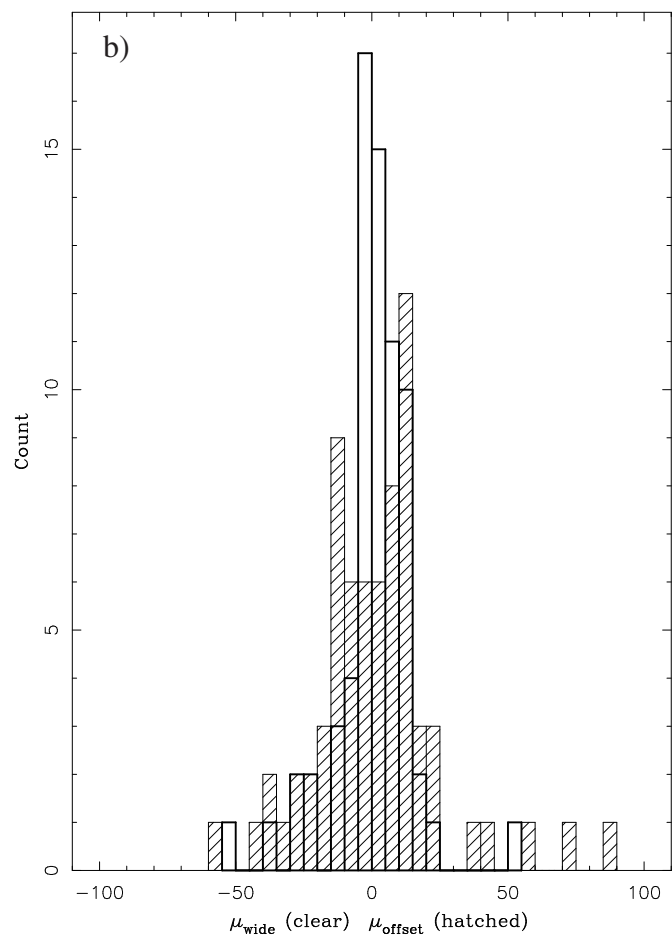
Fig. 7.— This plot shows the 95% cutoff value of  $P(V)$ , which is the value of  $P(V)$  which 95% of all distributions lie below. Samples of 30, 54, 100, 615, and 1230 galaxies were generated via equation 5 (thin lines) and 6 (thick lines). The value of  $\alpha$  for which these lines drop below a value of 0.05 is referred to as  $\alpha_{95}$ .  $\alpha_{95}$  represents the smallest amplitude of a sinusoidal anisotropy for which 95% of the distributions would be detected via the Kuiper Test. Notice the similar results for distributions generated by both equation 5 and equation 6.



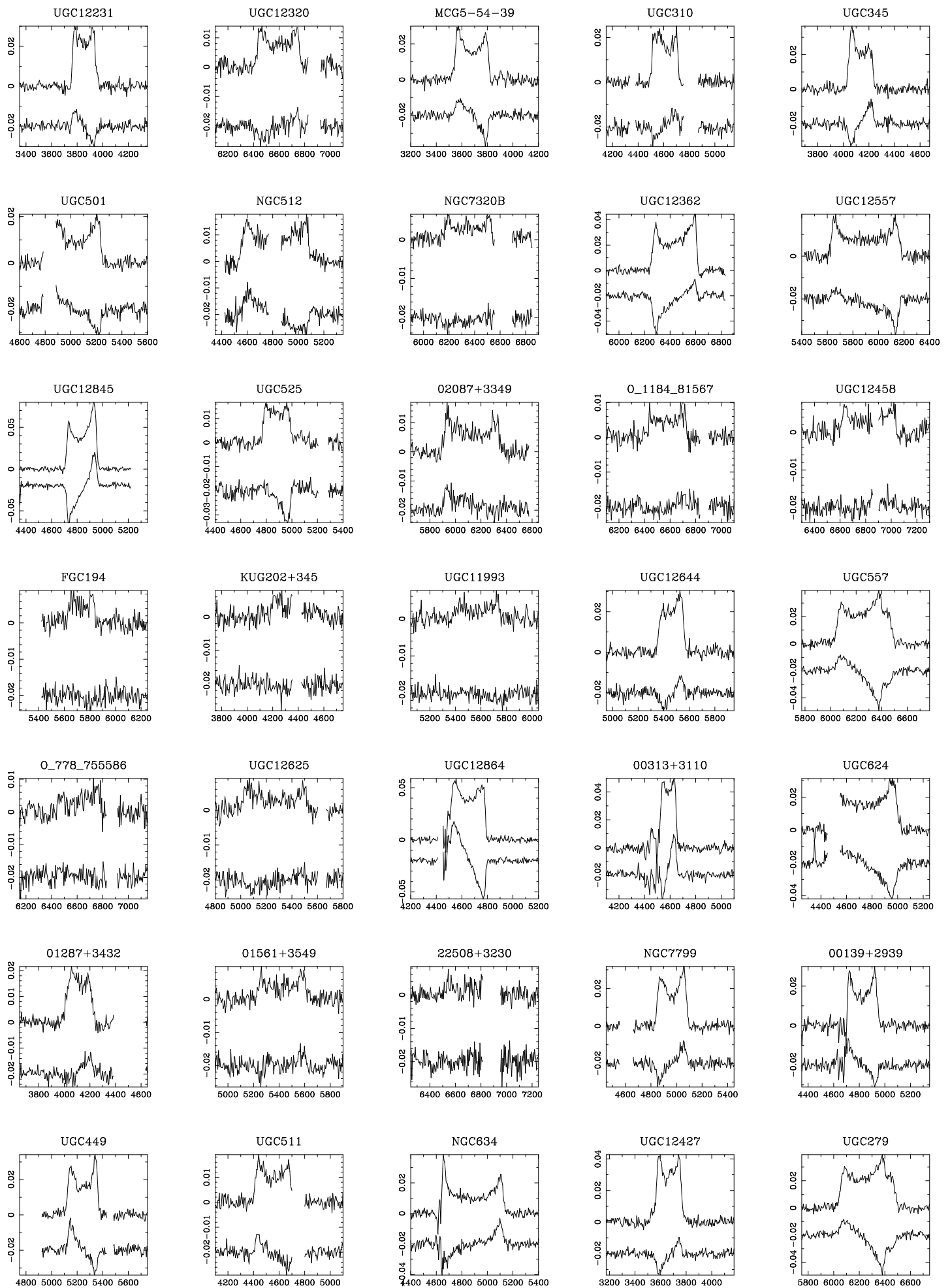
MAPS-PP Arecibo:  $\mu_{E-W}$  Distribution

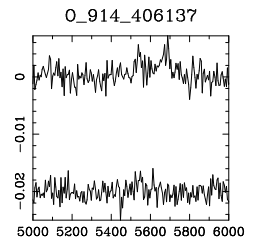
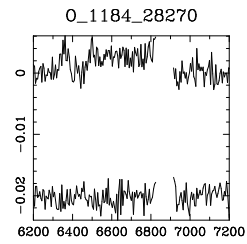
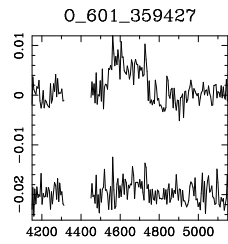
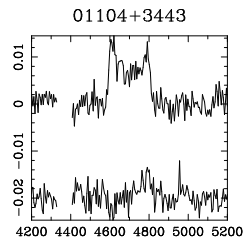
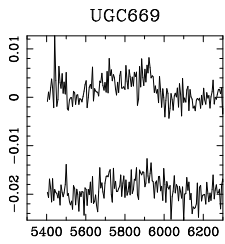
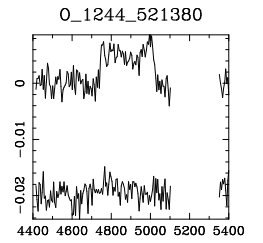
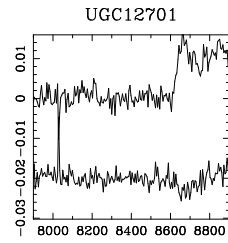
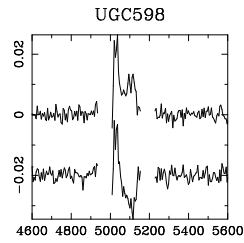
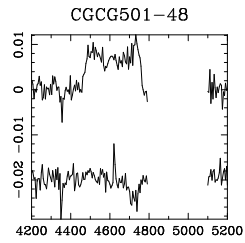
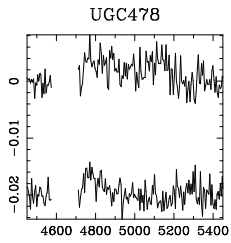
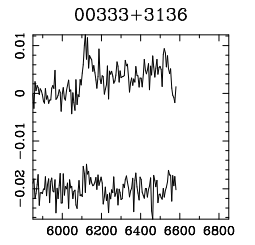
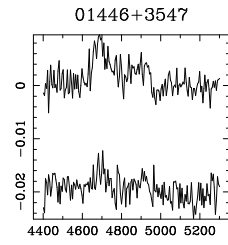
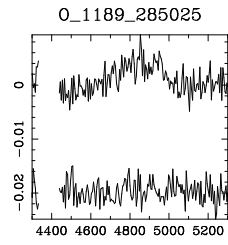
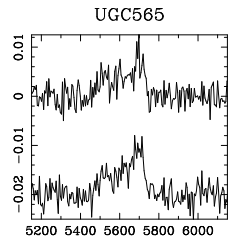
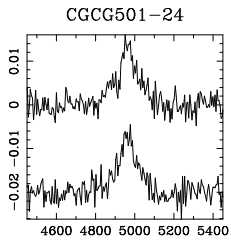
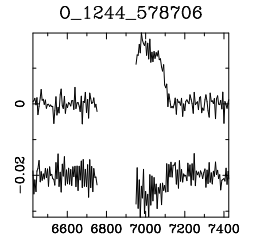
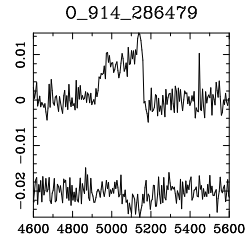
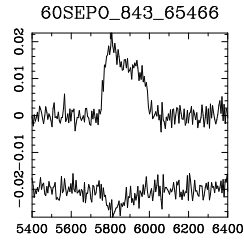
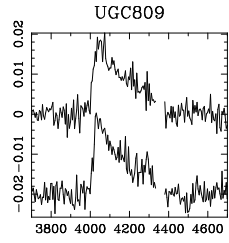
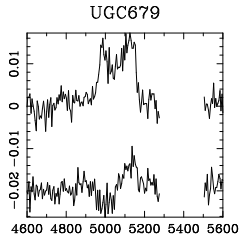
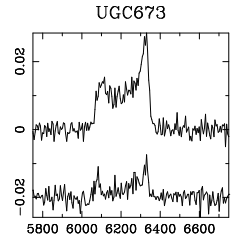
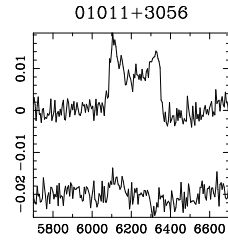
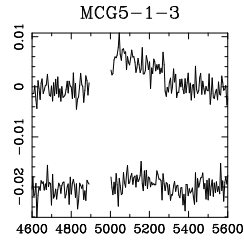
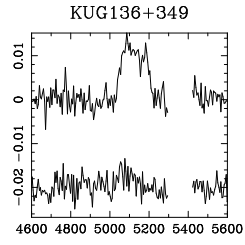
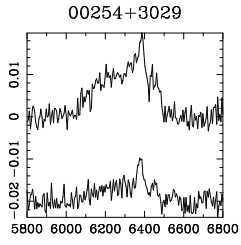
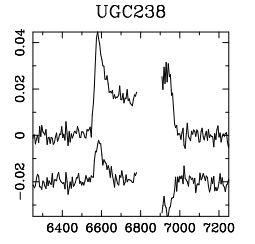
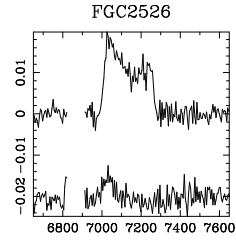
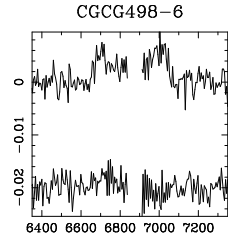
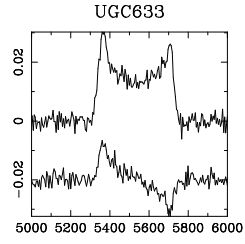
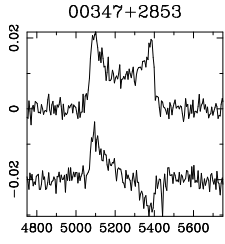
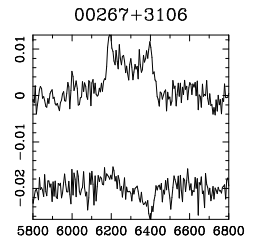
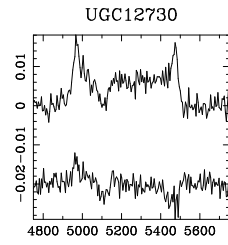
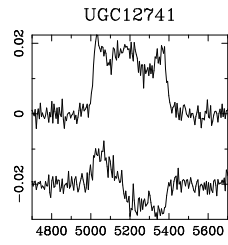
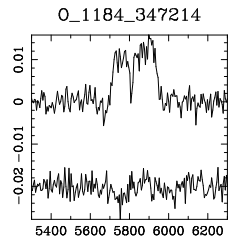
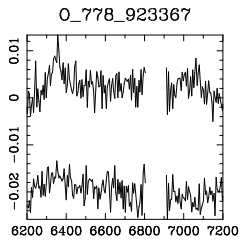


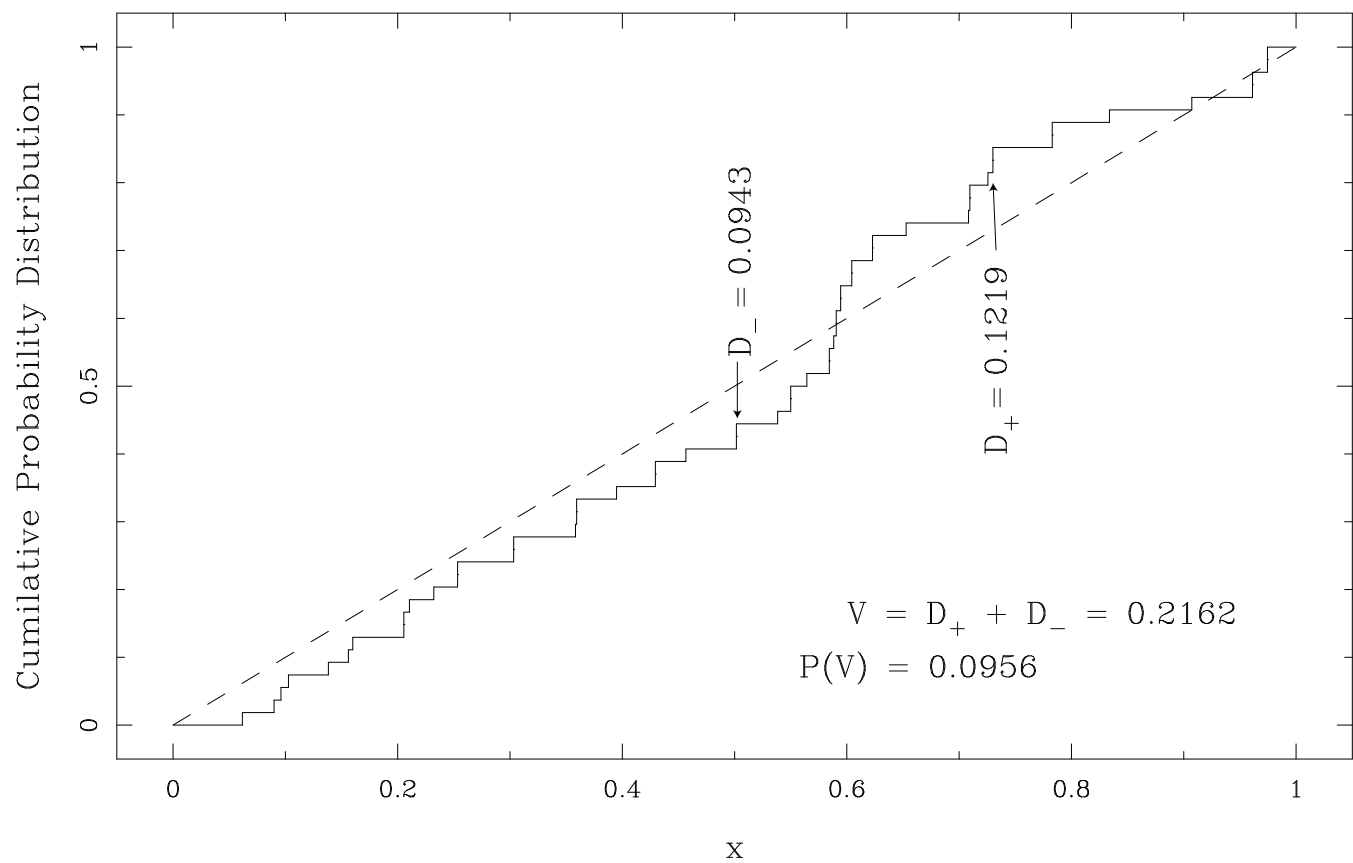
MAPS-PP Arecibo:  $\mu$  Uncertainty Measures

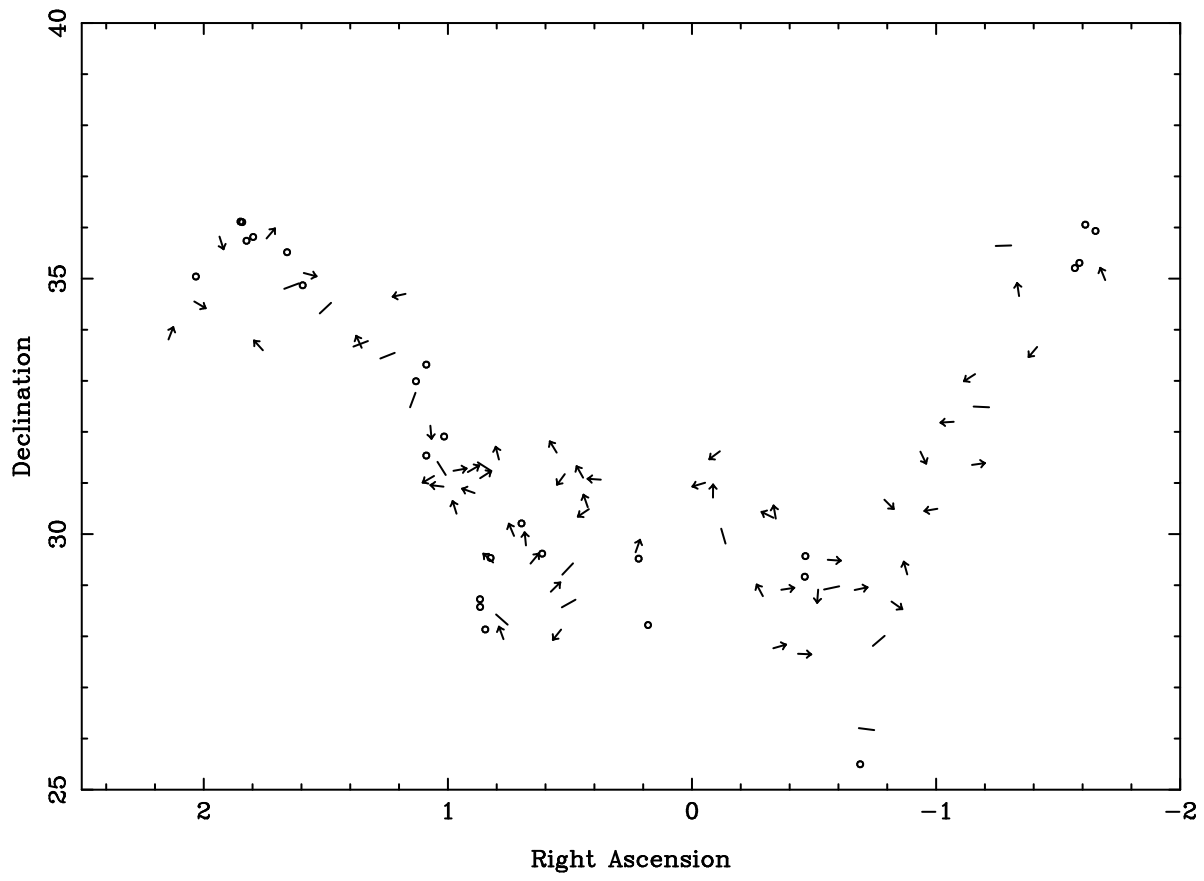




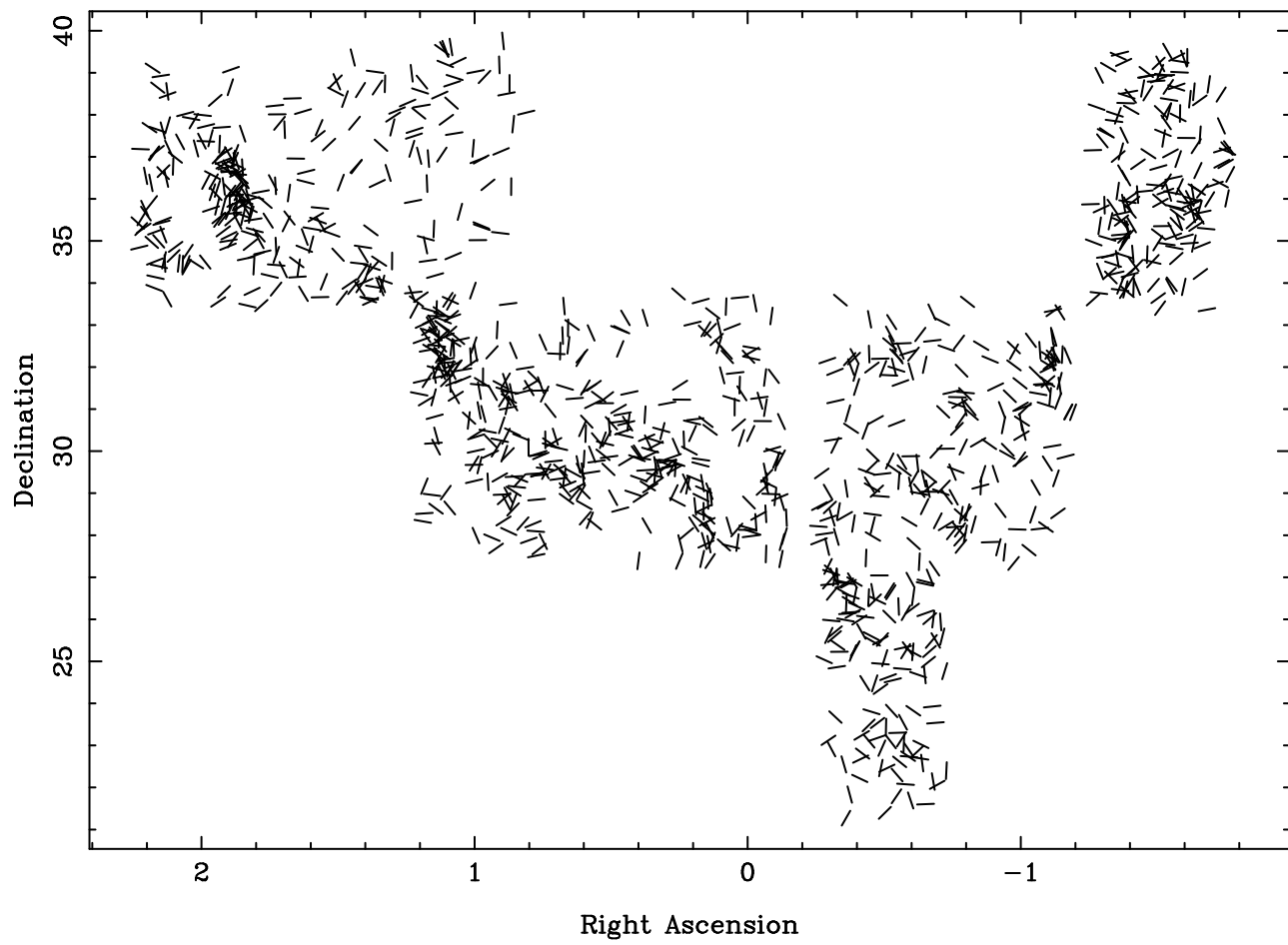








MAPS-PP Catalog (Major-Axis PA)



P(V) distribution versus Amplitude of Anisotropy

